RESOURCE AVAILABILITY

Lead Contact

Further information and requests for resources and reagents should be directed to and will be fulfilled by the lead contact, Prof Stephen Turner (stephen.j.turner@monash.edu).

Materials Availability

CCL5 mouse lines are available contingent on signing of appropriate Material Transfer Agreements between Institutions. All other materials are freely available.

Data and Code Availability

Hi-C and ATAC-seq data have been deposited at GEO and are publicly available as of the date of publication… Accession numbers are listed in the key resources table. All original code is publicly available as of the date of publication. RRIDs are listed in the key resources table. Any additional information required to reanalyse the data reported in this paper is available from the lead contact upon request

EXPERIMENTAL MODEL AND SUBJECT DETAILS

Mice

Ly5.2^{+} C57BL/6J, *Satb1*$^{m1Anu/m1Anu}$, and Ly5.1^{+} OT-I mice were bred and housed under specific-pathogen-free conditions at the Monash Animal Research Platform, with housing and experimental procedures approved by the Monash University Animal Ethics Committee. *Bach2*$^{fl/fl}$ x *Cd4Cre* mice were bred and housed under specific-pathogen-free conditions at the Department of Microbiology and Immunology Animal Facility at the University of Melbourne. All mice used were female, and aged 8-12 weeks old. For infection, mice were anaesthetised and infected i.n. with 10^4 p.f.u. of recombinant A/HKx31 virus engineered to express the $OVA_{257–264}$ peptide (x31-OVA) in the neuraminidase stalk. For adoptive transfer studies, CD45.1^{+} OT-I T cells were adoptively transferred into female CD45.2^{+} recipients.

Primary Cell Cultures

Naive CD8α+ CD44lo/int cells were sort-purified from C57BL/6J or Δ−5Kb and Δ−20Kb mice (8-12 weeks) (> 99% purity). Cultures were initiated by stimulating 3.3 × 105 T cells with plate-bound anti-CD3ε (10ug/ml), anti-CD28 (5ug/ml), and anti-CD11a (10ug/ml) antibodies, and cultured in the presence of IL-2 (10U/ml). Cells were cultured in 3ml RPMI, supplemented with 10% FCS (v/v), 2mM L-glutamine, and penicillin and streptomycin in 6-well plates,

before being expanded into T25 flasks (10mls media) after 72hrs, T75 flasks at 96hrs (20ml media). Cultures were harvested at 120hrs.

METHOD DETAILS

ATAC-seq

We used an ATAC-seq protocol adapted from (Buenrostro et al., 2013). Nuclei were extracted from 50,000 naive, effector or memory, sort-purified OT-1 cells and immediately resuspended in transposition reaction mix (Illumina Nextera DNA Sample Preparation Kit - Cat #FC121-1030) for 30 minutes at 37C. Transposed DNA was purified using a QIAGEN MinElute PCR Purification kit (Cat #28004), and amplified for 5 PCR cycles using PCR primer 1 (Ad1_noMX) and an indexed PCR primer. Aliquots of each amplicon were used as template in a real-time quantitative PCR for 20 cycles to determine the optimal cycle number for library amplification, with amplicons purified as previously. Library quality was determined using a Bioanalyzer (Agilent) to ensure that amplicons ranged between 50-200bp, and samples were subjected to paired-end sequencing on an Illumina Hiseq2500 instrument. Sequence data was mapped to UCSC mm10, then filtered for PCR duplicates and blacklisted regions, then shifted using Alignment Sieve (deepTools; (Ramirez et al., 2014)) and lastly peaks were called with MACS2 (https://github.com/macs3-project/MACS).

ChIP and FAIRE

Effector T cells were crosslinked with 0.6% formaldehyde for 10 min at RT. Following sonication, immune-precipitation was performed with anti-H3K4me3, H3K27me3 or HK3K27Ac ChIP-grade antibodies and Protein A magnetic beads (Millipore). FAIRE was performed on samples fixed and sonicated as per ChIP, with accessible chromatin extracted twice with phenol:chloroform:isoamyl (25:24:1) (Sigma). FAIRE enrichment was normalised against a total input for which reverse cross-linking had been performed. ChIP and FAIRE enrichment was measured using quantitative real-time PCR, with data normalised against a total input and no-antibody control. Primers used in these assays were reported previously (Russ et al., 2017).

Hi-C

Hi-C was performed as per Rao (Rao et al., 2014), with the following adjustments: Step 2 - cells were fixed with 1.5% formaldehyde for 10 min at RT. Step 7 - the nuclei extraction buffer contained 0.4% Igepal. Step 12 - restriction digestion was performed overnight with 400U

Mbo1 (NEB) in NEB buffer 2.1. Steps 28-35 were skipped. Step 54 - 2.5ul NEBNext Adapter for Illumina (cat # E7370) was used in place of Illumina indexed adapter, with ligation at 20C for 15 min, followed by addition of 3U USER enzyme and further incubation at 37C for 15min. Step 60 - samples were incubated at 95C for 10 min in a thermocycler, and beads were removed before final library amplification with NEBNext Multiplex Oligos for Illumina (cat # E7335S).

Data normalisation, Differential Loop calling, Gene assignment, MDS plots, GSEA

Raw Hi-C FASTQ files were aligned to the mouse genome (mm10 build), and binned Hi-C matrices generated using Juicer (Durand et al., 2016). Hi-C data was normalised and differential loops were called using multiHiCcompare (Stansfield et al., 2019). TADs were compared using TADCompare (Cresswell and Dozmorov, 2020). GSEA analysis was performed using the FGSEA package (https://www.biorxiv.org/content/10.1101/060012v3), with bubble plots made using a custom Tidyverse script (https://www.tidyverse.org/). MDS plots were generated using the edgeR MDS package (https://rdrr.io/bioc/edgeR/man/plotMDS.DGEList.html). Positioning of dots in MDS is directly proportional to sample similarity.

Data visualisation

Circos plots were generated using the ShinyCircos package (Yu et al., 2018). Enrichment plots were made using the deepTools2 package (Ramirez et al., 2016). All other figures were made using custom R codes and ggplots2 (Wickham, 2016).

Flow Cytometry

Single-cell suspensions from spleens, lymph nodes or bronchiolar lavage fluid (BAL) were stained with LIVE/DEAD Fixable Aqua Dead Cell Stain (Thermo Fischer Scientific) for 10 mins at room temperature. Cells were washed with MACS buffer (2mM EDTA, 2% BSA in PBS) prior to resuspension in antibody cocktail containing fluorochrome conjugated antibodies specific for CD4, CD8α, CD45.1, or CD44. For cytokine staining, cells were fix and permeabilised according to manufacturer's instructions (BD Biosciences) prior to staining with anti-CCL4 and CCL5 antibodies. Stained cells were washed twice with permeabilization buffer, and twice with MACS buffer before analysis. Samples were read with a FACSCanto II cytometers (BD Biosciences), and analysed using FlowJo software (Tree Star, Ashland, OR, USA).

QUANTIFICATION AND STATISTICAL ANALYSIS

In Figure 2, RNA-seq data are shown as the mean of 2 (memory) or 3 (naive and effector) biological replicate values, ± SEM. In Figure 3A, numbers of *cis* interactions unique to each differentiation state were determined by pairwise comparisons using multiHiCcompare (50Kb resolution, 0.05 FDR). 3B) GSEA analysis comparing genes connected by loops enriched in one condition over another (Y axis), against RNA-seq data derived from matching samples (Russ et al., 2014). Circle sizes reflect adjusted p values (-log10) and colour represents normalised enrichment score (NES), with red indicating enrichment versus the first RNA-seq condition listed in pairwise comparison, and blue indicating enrichment is the second RNA-seq condition listed. In Figure 4 enrichment of transcription factor binding at enhancers unique to naïve or effector (Russ et al., 2017) was performed using curated transcription factor ChIP-Seq data through the CistromeDB Toolkit with shading reflecting GIGGLE score (Zheng et al., 2019). In Figure 5 and 6, GSEA analysis comparing genes connected by loops gained in naïve Bach2$^{-/-}$ and *Satb1*$^{m1Anu/m1Anu}$ CD8^{+} T cells, respectively, relative to naïve WT CD8^{+} T cells against RNA-seq data derived from naïve and effector CTLs samples (datasets as described above). p values and normalised enrichment score (NES) are shown (Subramanian et al., 2005). All other Methods used to quantify and perform statistical analyses on data are described in figure legends.

REAGENT or RESOURCE	SOURCE	IDENTIFIER
Antibodies		
anti-CD45.1 (A20)	BD Biosciences	RRID:AB_395044
anti-CD8 (53-6.7)	BD Biosciences	RRID:AB_469400
anti-CD44 (IM7)	Biolegend	RRID:AB_830785
anti-CCL4	Thermo Fisher Scientific	RRID:AB_2551861
anti-CCL5	Biolegend	RRID:AB_2860706
Secondary Ab for CCL4	Thermo Fisher Scientific	RRID:AB_2534142

Bacterial and virus strains		
A/HKx31-OVA Influenza virus	Doherty Lab	(Jenkins et al., 2006)
Chemicals, peptides, and recombinant proteins		
Recombinant human IL-2		N/A
Ovalubumin 257-264 peptide (SIINFEKL)	Auspep	N/A
Critical commercial assays		
Fixation/Permeabilisation Solution Kit	BD Biosciences	Cat# 555028
NEBNext CHIP-seq Library Prep Master Mix Set for Illumina	New England BioLabs	Cat# NEB #E6240L
Deposited data		
WT Double Positive, Naive, Effector, Memory HiC data	This manuscript	Accession xxx
Naive Bach2-/- Hi-C data	This manuscript	Accession xxx
Naive Satb1$^{m1ANU/m1ANU}$ Hi-C data	This manuscript	Accession xxx
Naive, Effector, Memory ATAC-Seq data	This manuscript	Accession xxx
Experimental models: Organisms/strains		
OT-I Transgenic mouse strain		RRID:IMSR_JAX:003831
C57BL/6J		RRID:IMSR_JAX:000664
Ccl5 Δ-5	This manuscript	
Ccl5 Δ-20	This manuscript	
Satb1$^{m1ANU/m1ANU}$		(Koay et al., 2019)
Bach2fl/fl x CD4CRE		(Sidwell et al., 2020)

Software and algorithms		
Cistrome Toolkit		RRID:SCR_005396
Bedtools		RRID:SCR_006646
ggplot2		RRID:SCR_014601
MACS2		RRID:SCR_013291
R		RRID:SCR_001905
deepTools		RRID:SCR_016366
FlowJo v10	FlowJo	RRID:SCR_008520
MulitHiCcompare		RRID:SCR_022368
Tidyverse		RRID:SCR_019186
Juicer		RRID:SCR_017226
ShinyCircoss		RRID:SCR_022367

Buenrostro, J.D., Giresi, P.G., Zaba, L.C., Chang, H.Y., and Greenleaf, W.J. (2013). Transposition of native chromatin for fast and sensitive epigenomic profiling of open chromatin, DNA-binding proteins and nucleosome position. Nat Methods *10*, 1213-1218.

Cresswell, K.G., and Dozmorov, M.G. (2020). TADCompare: An R Package for Differential and Temporal Analysis of Topologically Associated Domains. Front Genet *11*, 158.

Durand, N.C., Shamim, M.S., Machol, I., Rao, S.S., Huntley, M.H., Lander, E.S., and Aiden, E.L. (2016). Juicer Provides a One-Click System for Analyzing Loop-Resolution Hi-C Experiments. Cell Syst *3*, 95-98.

Jenkins, M.R., Webby, R., Doherty, P.C., and Turner, S.J. (2006). Addition of a prominent epitope affects influenza A virus-specific CD8+ T cell immunodominance hierarchies when antigen is limiting. J Immunol *177*, 2917-2925.

Koay, H.F., Su, S., Amann-Zalcenstein, D., Daley, S.R., Comerford, I., Miosge, L., Whyte, C.E., Konstantinov, I.E., d'Udekem, Y., Baldwin, T.*, et al.* (2019). A divergent transcriptional landscape underpins the development and functional branching of MAIT cells. Sci Immunol *4*.

Ramirez, F., Dundar, F., Diehl, S., Gruning, B.A., and Manke, T. (2014). deepTools: a flexible platform for exploring deep-sequencing data. Nucleic Acids Res *42*, W187-191.

Ramirez, F., Ryan, D.P., Gruning, B., Bhardwaj, V., Kilpert, F., Richter, A.S., Heyne, S., Dundar, F., and Manke, T. (2016). deepTools2: a next generation web server for deep-sequencing data analysis. Nucleic Acids Res *44*, W160-165.
Rao, S.S., Huntley, M.H., Durand, N.C., Stamenova, E.K., Bochkov, I.D., Robinson, J.T., Sanborn, A.L., Machol, I., Omer, A.D., Lander, E.S., and Aiden, E.L. (2014). A 3D map of the human genome at kilobase resolution reveals principles of chromatin looping. Cell *159*, 1665-1680.
Russ, B.E., Olshanksy, M., Smallwood, H.S., Li, J., Denton, A.E., Prier, J.E., Stock, A.T., Croom, H.A., Cullen, J.G., Nguyen, M.L.*, et al.* (2014). Distinct Epigenetic Signatures Delineate Transcriptional Programs during Virus-Specific CD8(+) T Cell Differentiation. Immunity *41*, 853-865.
Russ, B.E., Olshansky, M., Li, J., Nguyen, M.L.T., Gearing, L.J., Nguyen, T.H.O., Olson, M.R., McQuilton, H.A., Nussing, S., Khoury, G.*, et al.* (2017). Regulation of H3K4me3 at Transcriptional Enhancers Characterizes Acquisition of Virus-Specific CD8(+) T Cell-Lineage-Specific Function. Cell Rep *21*, 3624-3636.
Sidwell, T., Liao, Y., Garnham, A.L., Vasanthakumar, A., Gloury, R., Blume, J., Teh, P.P., Chisanga, D., Thelemann, C., de Labastida Rivera, F.*, et al.* (2020). Attenuation of TCR-induced transcription by Bach2 controls regulatory T cell differentiation and homeostasis. Nat Commun *11*, 252.
Stansfield, J.C., Cresswell, K.G., and Dozmorov, M.G. (2019). multiHiCcompare: joint normalization and comparative analysis of complex Hi-C experiments. Bioinformatics *35*, 2916-2923.
Subramanian, A., Tamayo, P., Mootha, V.K., Mukherjee, S., Ebert, B.L., Gillette, M.A., Paulovich, A., Pomeroy, S.L., Golub, T.R., Lander, E.S., and Mesirov, J.P. (2005). Gene set enrichment analysis: a knowledge-based approach for interpreting genome-wide expression profiles. Proc Natl Acad Sci U S A *102*, 15545-15550.
Wickham, H. (2016). ggplot2 : Elegant Graphics for Data Analysis. In Use R!, (Cham, Springer International Publishing : Imprint: Springer,), pp. 1 online resource (XVI, 260 pages 232 illustrations, 140 illustrations in color.
Yu, Y., Ouyang, Y., and Yao, W. (2018). shinyCircos: an R/Shiny application for interactive creation of Circos plot. Bioinformatics *34*, 1229-1231.
Zheng, R., Wan, C., Mei, S., Qin, Q., Wu, Q., Sun, H., Chen, C.H., Brown, M., Zhang, X., Meyer, C.A., and Liu, X.S. (2019). Cistrome Data Browser: expanded datasets and new tools for gene regulatory analysis. Nucleic Acids Res *47*, D729-D735.

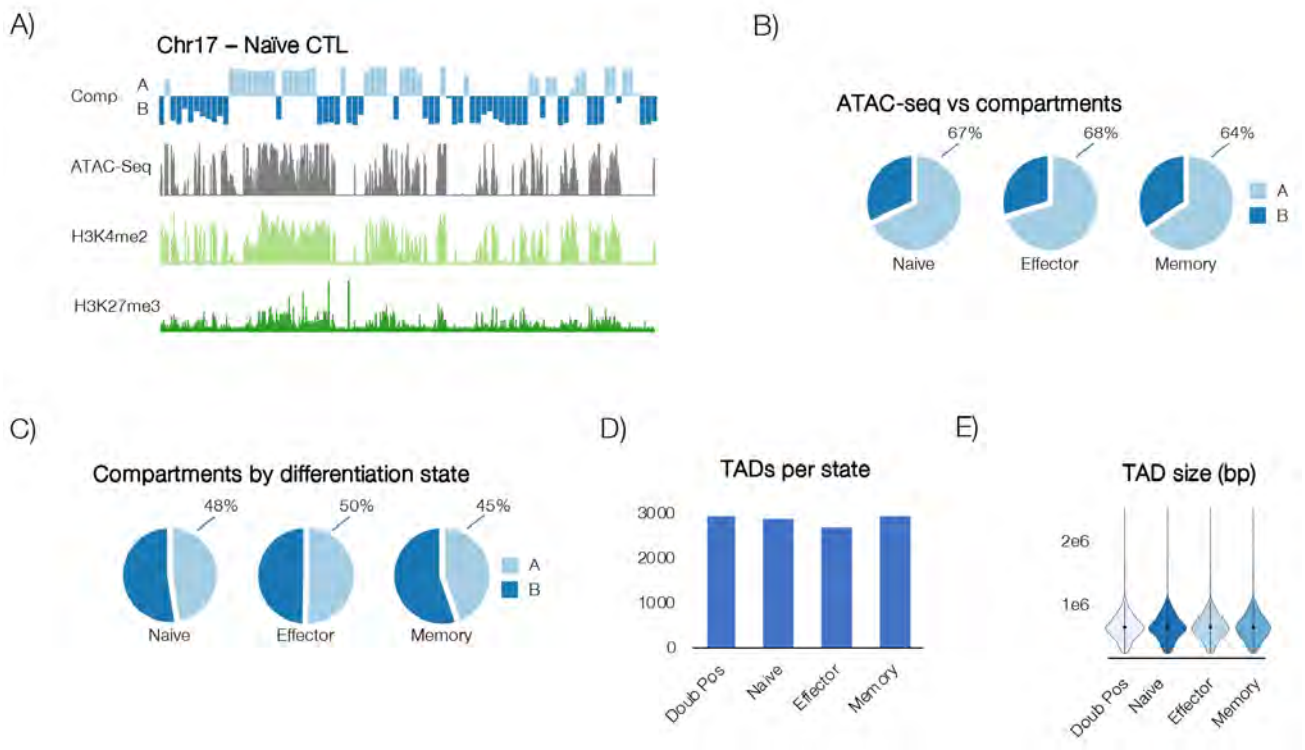

Supplementary Figure 1. Conservation of higher order chromatin structures during CTL differentiation. A) Genomic compartments broadly reflect chromatin state. Eigenvectors calculated at 1Mb resolution for chromosome 17 of naïve CTL, with A and B compartments shown in light blue and dark blue, respectively, compared with paired ATAC-seq (grey), H3K4me2 (light green) and H3K27me3 (dark green) ChIP-Seq data. B) Genome-wide overlap of open chromatin peaks (identified by ATAC-Seq) and A/B compartments shows that most open regions occur within the A compartment (indicated by percentage figures). C) Similar A/B compartment distribution between differentiation states. D) Average TAD number and size (E) was stable during differentiation of double positive to naïve and virus-specific effector and memory CTL.

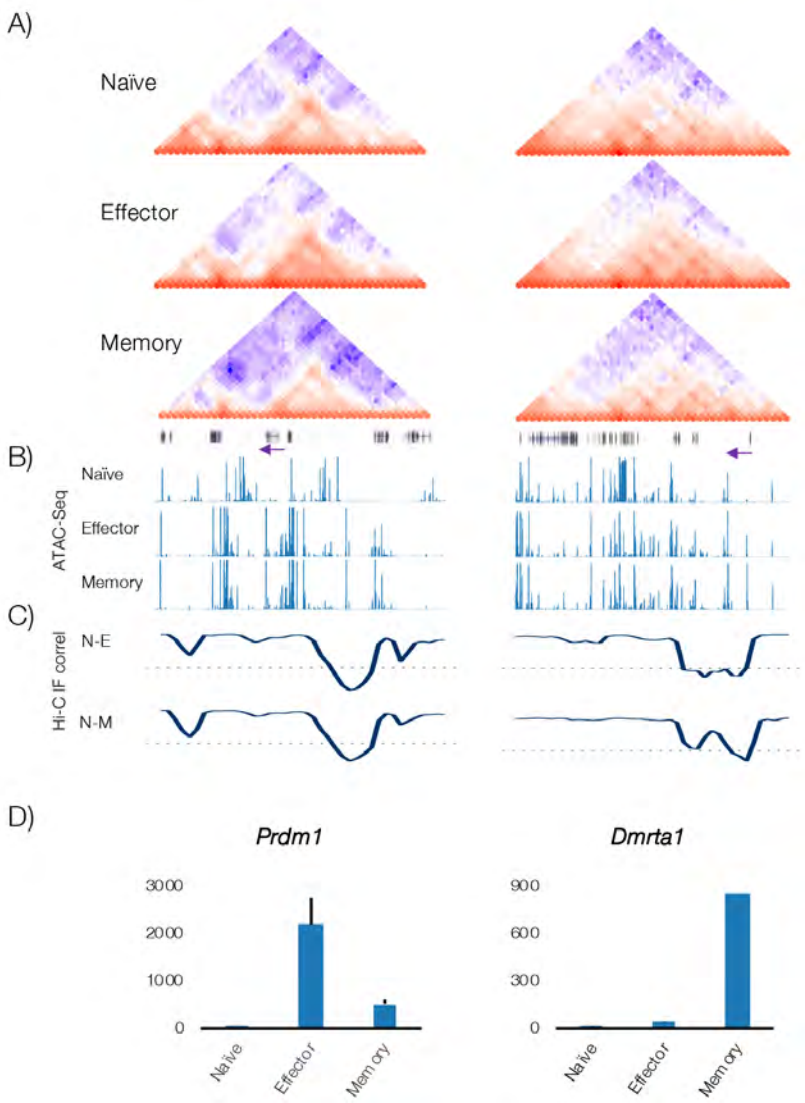

Supplementary Figure 2. A) Hi-C data (50Kb bins) normalised using ICED method showing interaction frequency at *Prdm1* and *Dmrta1* loci in naïve, effector and memory OT-1 CTLs. Track below memory panel shows genes, with purple arrow highlighting genes of interest and their direction of transcription. B) ATAC-Seq data for Naïve, effector and memory OT-1 CTLs. C) Pairwise correlation of binned interaction frequencies (50kb) for naïve and effector (N-E), and naïve and memory (N-M) samples, with dotted line indicating 0 on the y axis. D) Bottom panel shows normalised RNA-Seq counts (Russ *et al*, 2014).

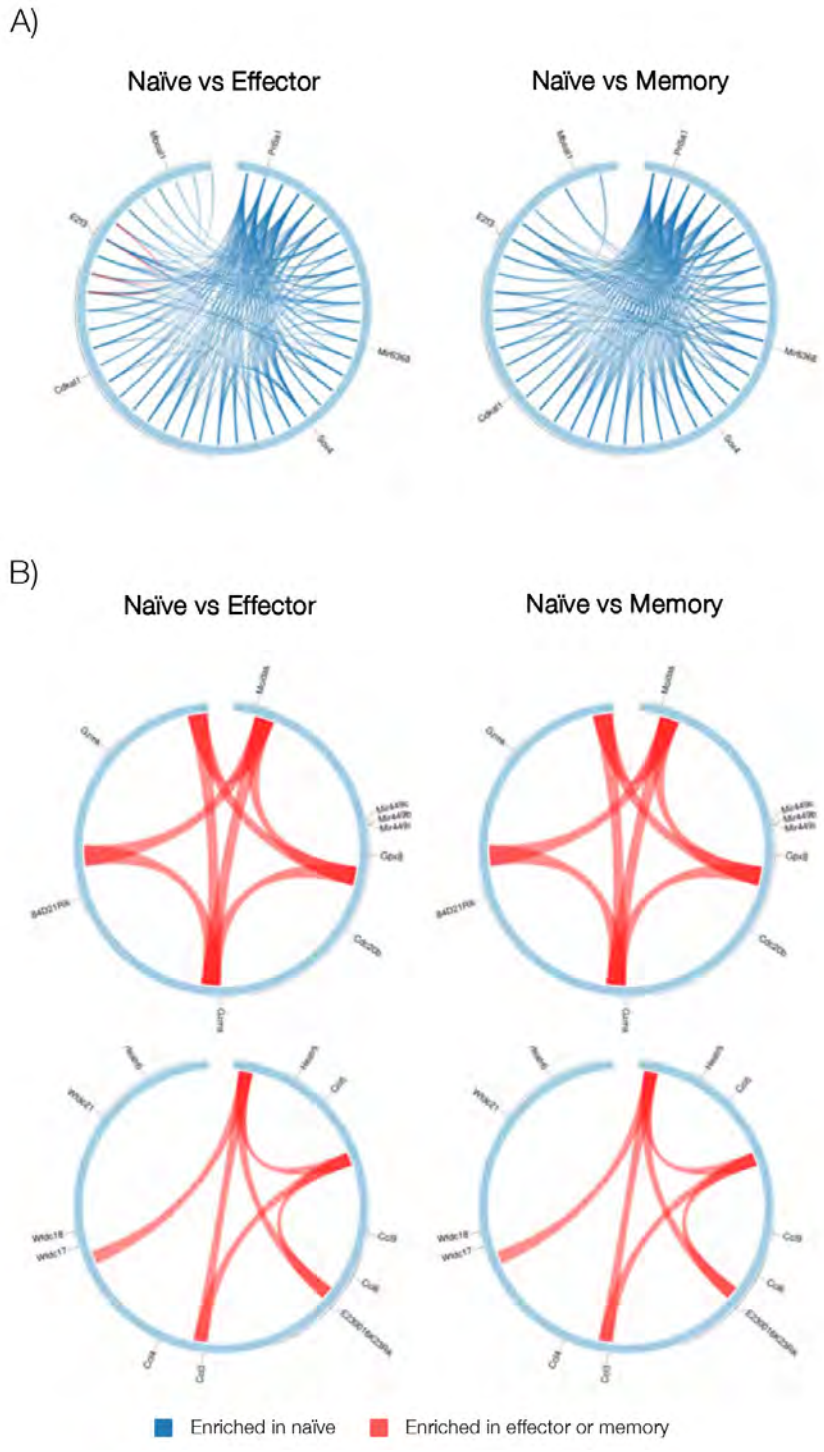

Supplementary Figure 3. Loss and gain of *cis* regulatory interactions underscores CTL differentiation state specific gene transcription profiles. A) Examples of loci where loops were largely lost upon differentiation (blue loops are present in naïve over effector or memory; red loops are gained on differentiation). B) Examples of loci where loops were largely gained upon differentiation.

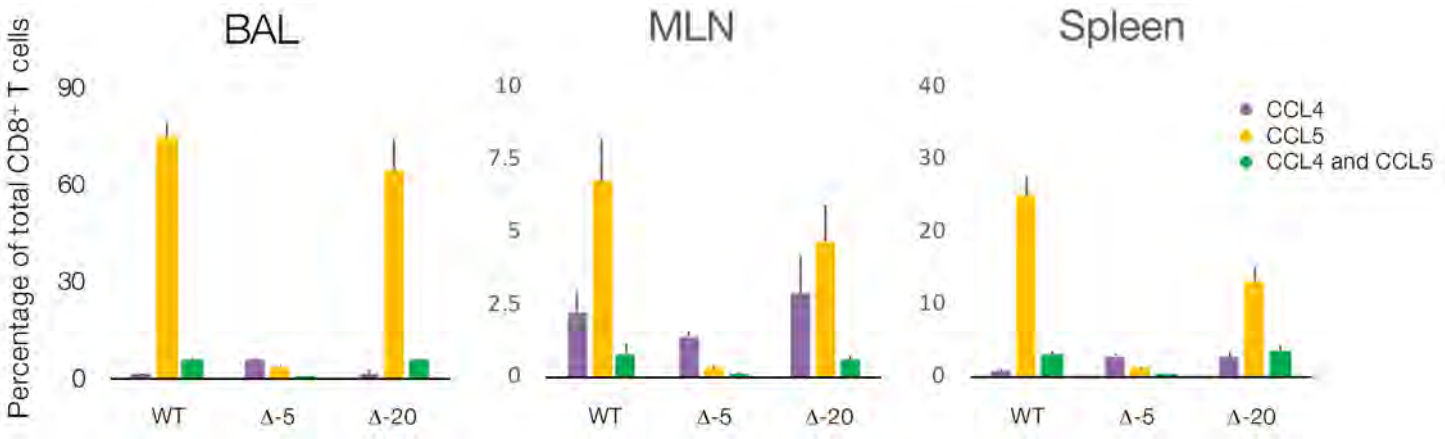

Supplementary Figure 4. Altered T cell chemokine expression in mice following deletion of cis interacting elements mapped by Hi-C. Percentage of $CD8^+$ and $CD4^+$ T cells expressing chemokines CCL4 and CCL5 in BAL, Spleen and MLN 10 days post challenge. WT (blue), -5 (red), -20 (green). Error bars are SEM. N=18-27 mice, across 3 separate experiments. % - p=<0.05 WT vs Δ-5; # - p=<0.05 WT vs Δ-20.